Luminescent kinetic characteristics of lead-containing aggregates dispersed in $Rb_{1-x}Cs_xCl$ (x = 0.05–0.2) matrices

2004 J. Phys.: Condens. Matter 16 483

(http://iopscience.iop.org/0953-8984/16/3/024)

INSTITUTE OF PHYSICS PUBLISHING JOURNAL OF PHYSICS: CONDENSED MATTER

J. Phys.: Condens. Matter **16** (2004) 483–490 PII: S0953-8984(04)63767-2

Luminescent kinetic characteristics of lead-containing aggregates dispersed in $Rb_{1-x}Cs_xCl$ (x = 0.05–0.2) matrices

S Myagkota[1], A Gloskovskii[1], R Gladyshevskii[1], A Voloshinovskii[1] and P Rodnyi[2]

[1] Ivan Franko National University of Lviv, 8 Kirila I Mefodiya Street, 79005 Lviv, Ukraine
[2] St Petersburg State Polytechnical University, Polytechnicheskaya 29, 195251, St Petersburg, Russia

E-mail: volosh@wups.lviv.ua and Rodnyi@tuexph.stu.neva.ru

Received 19 May 2003
Published 9 January 2004
Online at stacks.iop.org/JPhysCM/16/483 (DOI: 10.1088/0953-8984/16/3/024)

Abstract

The luminescent kinetic parameters of $CsPbCl_3$ nanocrystals dispersed in matrices of the solid solutions $Rb_{1-x}Cs_xCl$ (x = 0.05–0.2) were studied under pulse synchrotron radiation excitation. Formation of $CsPbCl_3$ nanocrystals is confirmed by the manifestation of the quantum size effect, which shows itself as a blue-shift of the exciton luminescence maximum and an essential shortening of the luminescence decay time for $CsPbCl_3$ nanocrystals as compared to that for an excitonic luminescence of a bulk single crystal $CsPbCl_3$. For the first time, using the atomic force microscopy method, the lead-containing nanocrystals embedded in a matrix of the $Rb_{0.95}Cs_{0.05}Cl$ solid solution were directly observed.

1. Introduction

Along with the well-known semiconducting nanocrystals of the CdS, CdSe, CuCl, PbI_2 type, recently the ionic lead-containing crystals of the $CsPbX_3$ (X = Cl, Br, I) type have been extensively studied. Some of them are characterized by a high intensity of the luminescence with short decay times (tens of picoseconds) [1]. Such luminescent parameters make these materials promising for use in development of fast detectors of high-energy irradiation as well as optoelectronics devices [2].

The $CsPbX_3$ (X = Cl, Br, I) nanocrystals are formed in insulating halide matrices with different crystal structures activated by the lead or caesium ions as the result of a prolonged (10–100 h) high-temperature (150–250 °C) annealing. Formation of these nanocrystals has been confirmed by the manifestation of the quantum size effect in their spectral luminescent

characteristics [1–5]. The high efficiency of the luminescence method for identification of the crystal type and nanocrystal sizes in the insulator matrix has been analysed in [6].

Lead-containing nanocrystals formed in matrices with the CsCl crystal structure were directly observed only in studies of the surface for $CsX–PbX_2$ (X = Cl, Br, I) thin films by the atomic force microscopy (AFM) method [7–9].

In present paper we study the luminescent kinetic characteristics of the $CsPbCl_3$ nanocrystals embedded in the matrix in $Rb_{1-x}Cs_xCl$ ($x = 0.05$–0.2) solid solutions. The crystal structure of $Rb_{1-x}Cs_xCl$ ($x = 0.05$–0.2) solid solutions is of the NaCl type, since the content of CsCl in $Rb_{1-x}Cs_xCl$ is less than $x = 0.33$. According to the results of the theoretical calculations, the structure type of the solid solution $A_{1-x}B_xX$ is the same as that of the major component AX if the content of the BX impurity is less than $x = 0.33$ [10]. The AFM method was used for the study of lead-containing nanocrystals dispersed in the matrices of the $Rb_{1-x}Cs_xCl$ ($x = 0.05$–0.2) solid solutions. In these studies the freshly cleaved crystal surfaces are explored which provides more advantages than thin film studies [7–9] where the observation of nanocrystals are distorted by the thin film structure.

Let us note that the formation of $CsPbCl_3$-type nanocrystals embedded in a crystalline structure of NaCl type has not been observed yet. Only for NaCl crystals activated by lead was it established that the increase of the storage time of the crystal or annealing temperature as well as the impurity content leads to the formation of Pb-containing aggregates of $PbCl_2$-type embedded in the NaCl matrix [11].

2. Experiment

The $Rb_{1-x}Cs_xCl$–Pb ($x = 0.05$–0.2) crystals ($C_{Pb} = 1$ mol% in the melt) were grown by the Stockbarger method in two stages. First the $Rb_{1-x}Cs_xCl$ ($x = 0.05$–0.2) crystal matrix, and then the $Rb_{1-x}Cs_xCl$–Pb crystal were grown. In order to form the $CsPbCl_3$ nanocrystals dispersed in the $Rb_{1-x}Cs_xCl$ ($x = 0.05$–0.2) matrix, the $Rb_{1-x}Cs_xCl$–Pb ($x = 0.05$–0.2) crystals were subjected to a prolonged (100 h) high-temperature ($T = 200\,^{\circ}C$) annealing.

The luminescent kinetic characteristics of the crystals were measured by the time resolved spectroscopy methods at the SUPERLUMI station of HASYLAB at DESY (Hamburg, Germany). The crystal was excited by the synchrotron radiation passed through a normal incidence 2 m vacuum monochromator (the spectral width of the slit was about $\sim$0.2 nm). The luminescence of the crystal located on the crystal holder of a helium cryostat was detected by a photomultiplier through a secondary monochromator (B&M trademark). The luminescence decay kinetics was studied under pulsed synchrotron excitation (the pulse duration was $\approx$0.12 ns, the repetition period was 480 ns) in the statistical single-photon counting regime with time-to-amplitude conversion. The experimental set-up provided the registration of the synchrotron excitation pulse as the profile with the decay time constant of 0.4 ns. Actual luminescence decay times were determined taking into account the excitation pulse shape and using the deconvolution procedure. According to [12], the iteration method used for the evaluation of one-exponent parameters of the decay time curve gives a satisfactory accuracy of approximation. The minimal time constant that can be estimated by this procedure is 0.15 ns. The luminescence spectra were measured within a time window $\Delta t = 5$ ns just after the synchrotron excitation pulse. The detailed description of experimental set-up has been presented in [13].

The topology of the cleavage surface of $Rb_{0.95}Cs_{0.05}Cl$–Pb crystal was explored by the using the AFM technique.

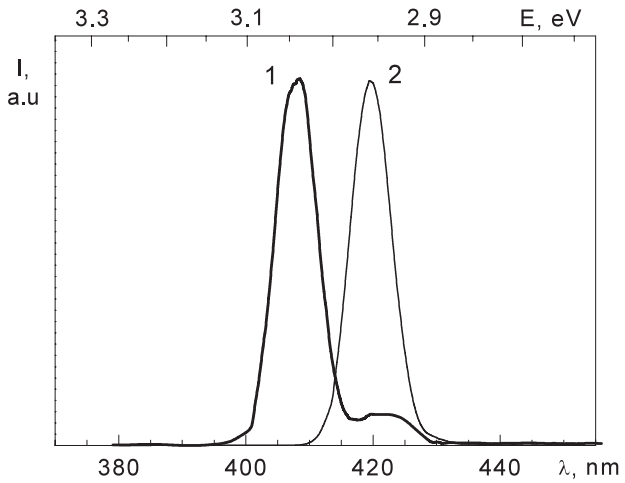

Figure 1. The luminescence spectrum of the $CsPbCl_3$ nanocrystals in $Rb_{0.95}Cs_{0.05}Cl$–Pb crystal (curve 1) excited in the matrix transparency region ($\lambda_{exc} = 310$ and 240 nm) and the luminescence spectrum of the $CsPbCl_3$ bulk single crystal excited at $\lambda_{exc} = 310$ nm (curve 2). $T = 10$ K.

3. Experimental results and discussion

The photoluminescence spectra of the $Rb_{0.95}Cs_{0.05}Cl$–Pb crystal, excited in the matrix transparency region ($\lambda_{exc} = 310$ and 240 nm) beyond the absorption bands of single lead centres, and the luminescence spectrum of the $CsPbCl_3$ single crystal are shown in figure 1.

The relatively narrow emission band with the FWHM $\Delta H = 0.04$ eV peaked at $\lambda_{max} = 408.0$ nm (figure 1, curve 1) of the $Rb_{0.95}Cs_{0.05}Cl$–Pb crystal is similar to the free exciton emission band of the $CsPbCl_3$ single crystal ($\lambda_{max} = 419.6$ nm, $\Delta H = 0.025$ eV) (figure 1, curve 2), the spectral position of which does not depend on the wavelength of the excitation light. Such a similarity of the spectral characteristics indicates that lead-containing aggregates of the $CsPbCl_3$ type are formed in the $Rb_{0.95}Cs_{0.05}Cl$–Pb crystal during high-temperature annealing. The intensity of luminescence for lead-containing aggregates of the $CsPbCl_3$ type is comparable with that of $CsPbCl_3$ single crystal. A high quantum yield ($B = 0.5$ at $T = 100$ K) for the luminescence of $CsPbCl_3$ single crystal has been determined in [14].

Formation of such aggregates in the $Rb_{1-x}Cs_xCl$–Pb ($x = 0.05$–0.2) crystalline matrices, where the Rb^+, Cs^+ ions and the impurity ion Pb^{2+} are characterized by a sixfold surrounding of Cl^- anions, seems logical, since the formation of the $[PbCl_6]^{4-}$ octahedron does not require any structural reconstruction. In the crystalline matrices of the CsCl type, the eightfold surrounding of the Cl^- anions must be changed to a sixfold one to create the cluster in the form of a $CsPbCl_3$ molecule. The $[PbCl_6]^{4-}$ octahedron is the basis of a $CsPbCl_3$ molecular cluster; therefore its presence in the matrix assists in formation of the nanocrystals and microcrystals of the $CsPbCl_3$ type in the $Rb_{1-x}Cs_xCl$–Pb crystals. Also, the presence of the charge-compensation vacancy v_c^- next to the activator Pb^{2+} ion facilitates the Pb^{2+} ion mobility with further formation of the lead-containing aggregates.

The blue-shift of the emission band maximum of the $CsPbCl_3$ nanocrystals in the $Rb_{0.95}Cs_{0.05}Cl$ matrix ($\lambda_{max} = 408.0$ nm) relatively to the position of the maximum of the free exciton emission band of the $CsPbCl_3$ single crystal by $\Delta E = 84$ meV can be interpreted as a manifestation of the quantum size effect. Using the relation between the magnitude of the

blue-shift and the average radius R_{QD} of the nanocrystal [15]

$$\Delta E = \frac{\hbar^2 \pi^2}{2\mu R_{QD}^2}, \tag{1}$$

where $\mu = 0.65\, m_0$ [16, 17] is the exciton reduced mass for the $CsPbCl_3$ single crystal (m_0 is the mass of a free electron), we determined the average radius of the $CsPbCl_3$-type nanocrystals dispersed in the $Rb_{0.95}Cs_{0.05}Cl$ matrix ($R_{QD} \approx 3$ nm). According to theoretical calculations, the quantum size effect shows itself in aggregates when $R_{QD} < 10r_{ex}$ [18]. Taking into account the numerical value of the exciton radius ($r_{ex} = 9.8$ Å [17] for $CsPbCl_3$), the value obtained for the average radius of the nanocrystals R_{QD} meets the condition for the manifestation of the quantum size effect.

The broadening of the FWHM of the luminescence band of the $CsPbCl_3$ aggregates dispersed in the $Rb_{0.95}Cs_{0.05}Cl$ matrix as compared to that of the $CsPbCl_3$ single crystals can be explained by formation of $CsPbCl_3$ nanocrystals of different sizes, embedded in the $Rb_{0.95}Cs_{0.05}Cl$ matrix.

The average sizes of the $CsPbCl_3$ nanocrystals formed during the similar high-temperature annealing in the $Rb_{0.95}Cs_{0.05}Cl$–Pb ($C_{Pb} = 1$ mol%) and CsCl–Pb ($C_{Pb} = 1$ mol%) crystals [19] are $R_{QD} \approx 3$ and 4.7 nm, respectively. This relation between the nanocrystal dimensions in the $Rb_{0.95}Cs_{0.05}Cl$ and CsCl matrices is explained by the fact that the probability of the $CsPbCl_3$ nanocrystal formation in the $Rb_{0.95}Cs_{0.05}Cl$ matrix is decreased, since the number of Cs^+ ions in the compound is decreased. On the other hand, with increasing of the Cs^+ ion number in the $Rb_{1-x}Cs_xCl$ crystalline solution from $x = 0.05$ to 0.2, the $CsPbCl_3$ nanocrystal size in the $Rb_{0.8}Cs_{0.2}Cl$ matrix becomes larger than in the $Rb_{0.95}Cs_{0.05}Cl$ matrix. Really, the average radius of the $CsPbCl_3$ nanocrystals formed in the $Rb_{0.8}Cs_{0.2}Cl$–Pb crystal upon high-temperature annealing similar to that in the case of $Rb_{0.95}Cs_{0.05}Cl$–Pb equals 4.7 nm. The luminescence maximum of the $CsPbCl_3$ nanocrystals in the $Rb_{0.8}Cs_{0.2}Cl$ matrix with $\lambda_{max} = 415$ nm is shifted to the red side relatively to the luminescence maximum of $\lambda_{max} = 408$ nm for the $CsPbCl_3$ nanocrystals dispersed in $Rb_{0.95}Cs_{0.05}Cl$. Coincidence of the values of the average radii of the $CsPbCl_3$ nanocrystals formed in $Rb_{0.8}Cs_{0.2}Cl$–Pb ($C_{Pb} = 1$ mol%) and in CsCl–Pb ($C_{Pb} = 1$ mol%) after identical high-temperature annealing procedures indicates that the slowing down of the $CsPbCl_3$ nanocrystal formation due to the reduced number of Cs ions in $Rb_{0.8}Cs_{0.2}Cl$ (as compared to that in CsCl) is compensated by the presence of the $[PbCl_6]^{4-}$ octahedrons in the $Rb_{0.8}Cs_{0.2}Cl$ matrix that accelerates it.

Conclusions about the manifestation of the quantum size effect of the $CsPbCl_3$ nanocrystals are confirmed by the luminescence decay kinetics studies. The luminescence decay time of the $CsPbCl_3$ nanocrystals, dispersed in $Rb_{0.95}Cs_{0.05}Cl$–Pb crystals, excited in the matrix transparency region, is described by an exponent with a decay time $\tau = 0.15$ ns, whereas the kinetics of the luminescence decay in the $CsPbCl_3$ single crystal, excited in the same spectral range, is described by the exponent with the decay time $\tau = 0.48$ ns (figure 2, curves 1 and 2, respectively). Thus, the main decay time for the nanocrystal luminescence is essentially shorter than the one for the excitonic luminescence of a $CsPbCl_3$ bulk crystal. Shortening of the luminescence decay time in the nanocrystals gives more evidence for the manifestation of the quantum size effect. In reality, the luminescence decay time of the nanocrystals can be less than 0.15 ns, which is the time limit of our set-up.

Along with the quantum size effect that influences the luminescent parameters, the matrix causes a hydrostatic pressure on the nanocrystals. This pressure arises due to the difference between the linear thermal expansion coefficients of the matrix and of the nanocrystals, as well as due to certain stress acting on the $CsPbCl_3$ nanocrystals upon their embedding into a matrix.

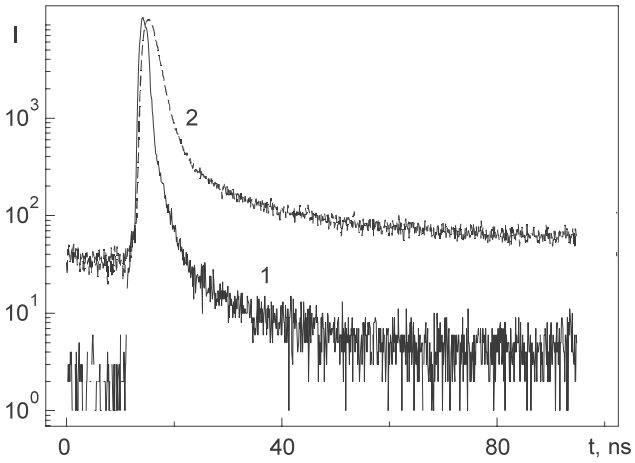

Figure 2. Luminescence decay kinetics curves of $CsPbCl_3$ nanocrystal dispersed in $Rb_{0.95}Cs_{0.05}Cl$ matrix (curve 1) excited in the transparency region of the $Rb_{0.95}Cs_{0.05}Cl$ matrix ($\lambda_{exc} = 330$ nm) and $CsPbCl_3$ single crystals (curve 2) ($\lambda_{exc} = 330$ nm). $T = 10$ K.

The linear thermal expansion coefficient for $CsPbCl_3$ single crystal is not determined. For the estimation of the $Rb_{0.95}Cs_{0.05}Cl$ matrix pressure use of the linear thermal expansion coefficient for TlCl crystal (2.99×10^{-5} K^{-1} [20]) is proposed, since TlCl crystals possess physical properties similar to those of $CsPbCl_3$ crystal due to the isoelectronic configurations of Tl^+ and Pb^{2+} ions and also owing to the nearest environments for these ions in corresponding compounds having the same symmetry [21]. The analysis conducted on the data on RbCl and KCl crystals represented in [22] enabled us to estimate the value of the linear thermal expansion coefficient α for $Rb_{0.95}Cs_{0.05}Cl$ matrix as being equal to 4.0×10^{-5} K^{-1} which is greater than the analogous value for TlCl crystal [20]. Thus, it could be concluded that $CsPbCl_3$ nanocrystals undergo the some compression in the $Rb_{0.95}Cs_{0.05}Cl$ matrix upon cooling of $Rb_{0.95}Cs_{0.05}Cl$–Pb crystal from $T = 500$ K (the temperature of $CsPbCl_3$ nanocrystal creation) down to $T = 10$ K (the temperature of the luminescent measurements).

In the presence of such stress, the unit cell constants of the $CsPbCl_3$ nanocrystals are decreased, but the excitonic reflectance peak and the intrinsic emission spectrum of the nanocrystal are shifted to the red region, which is uncharacteristic for several other crystals. Such an anomalous shift in $CsPbCl_3$ is clearly seen in the temperature dependences of the spectral position of the excitonic reflectance peak and of the resonance excitonic luminescence band of a $CsPbCl_3$ single crystal in the 77–4.2 K temperature range. That is, when temperature is lowered and the lattice constant is decreased, the excitonic reflectance peak and the luminescence band of the $CsPbCl_3$ single crystal are shifted to lower energies [17]. Hence, the hydrostatic pressure on the nanocrystals veils the manifestation of the quantum size effect for $CsPbCl_3$ nanocrystals.

The hydrostatic pressure on $CsPbCl_3$ nanocrystals embedded into the matrix of $Rb_{1-x}Cs_xCl$ ($x = 0.05$–0.2) solid solution due to geometrical incommensurability of the lattice constants of the nanoparticles and matrix should also be considered. For this purpose the value of the unit cell constant for the $Rb_{0.95}Cs_{0.05}Cl$ matrix has been estimated taking into account the existence of a continuous series of RbCl–CsCl solid solutions [23]. This enabled us to determine the unit cell constant for $Rb_{0.95}Cs_{0.05}Cl$ solid solution as $a = 6.40$ Å using the values of analogous parameters for RbCl and CsCl crystals ($a = 4.11$ and 6.56 Å respectively).

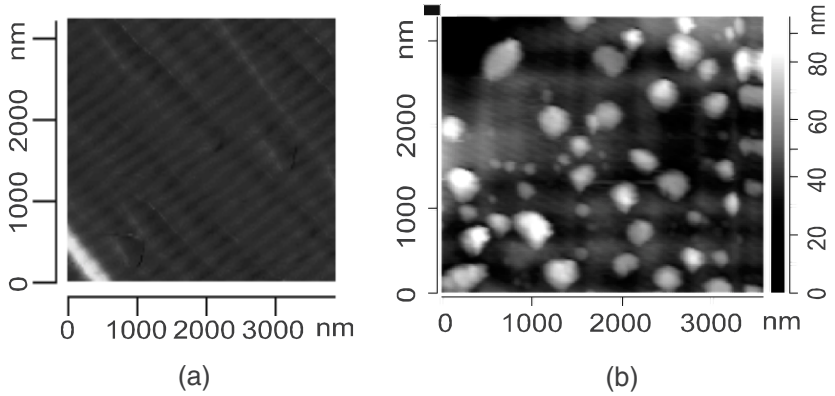

Figure 3. An AFM picture of the cleavage surface of $Rb_{0.95}Cs_{0.05}Cl$ matrix (a) and $Rb_{0.95}Cs_{0.05}Cl$–Pb crystal (b).

Since the value of the unit cell constant for the high-temperature cubic phase of $CsPbCl_3$ single crystal ($a = 5.6$ Å [16]) is smaller than the one estimated for $Rb_{0.95}Cs_{0.05}Cl$ ($a = 6.40$ Å), the unit cell of $CsPbCl_3$ nanocrystals embedded in $Rb_{0.95}Cs_{0.05}Cl$ matrix undergoes stretching under the condition of parallel orientation for the unit cells of the matrix and nanocrystal. Due to such stretching the unit cell constant for $CsPbCl_3$ nanocrystal increases but the exciton reflection peak and the intrinsic emission spectrum of the nanocrystal are shifted to the short-wave region as was mentioned above.

Thus, we did not exclude the possibility that the effect of hydrostatic pressure (caused by the difference of the linear thermal expansion coefficients for $Rb_{1-x}Cs_xCl$ matrices and $CsPbCl_3$ nanocrystals) is compensated by the stretching of $CsPbCl_3$ nanocrystals in $Rb_{1-x}Cs_xCl$ ($x = 0.05$–0.2) matrices. Possibly, this circumstance enables the quantum confinement effect to be revealed without the effect of hydrostatic pressure as the high-energy shift of the exciton emission band for $CsPbCl_3$ nanocrystal. Therefore, the study of the quantum confinement effect for $CsPbCl_3$ nanocrystals embedded in $Rb_{1-x}Cs_xCl$ ($x = 0.05$–0.2) matrices is rather more attractive than the study of the one for $CsPbCl_3$ nanocrystals embedded in a CsCl matrix.

Using the AFM method we explored the topology of the cleavage planes of the $Rb_{0.95}Cs_{0.05}Cl$–Pb crystal (figure 3). A spatial picture of Pb-based nanocrystals on the cleavage planes of the $Rb_{0.95}Cs_{0.05}Cl$–Pb crystal is shown as figure 4. The lateral size of $CsPbCl_3$ nanocrystals is essentially distorted by a tip convolution effect. This effect appears due to the macroscopic size of the scanning tip (≈50 nm). Therefore, only a height value should be taken as a nanocrystal size. The vertical scan resolution was 0.5 nm. Finally, the size of $CsPbCl_3$ nanocrystals may be estimated in the 4–30 nm region.

According to the AFM data (namely the statistical size distribution for $CsPbCl_3$ nanocrystals), the most probable value for the radius of Pb-based nanocrystals is $R_{QD} \approx 10$ nm (figure 5). The difference between the calculated value (3.0 nm) for the averaged radius of $CsPbCl_3$ nanocrystals obtained by using expression (1) and the one estimated by the AFM method (10 nm) can be explained taking into account that the surface image obtained by the AFM method represents nanocrystals covered by a layer of distorted matrix. The distortion of the matrix layer around the embedded nanocrystal is caused by the difference in size and symmetry of the unit cells of the matrix and the nanocrystal. The thickness of the distorted matrix layer equals the size of 5–10 unit cells and amounts to ≈3–6 nm, since the estimated

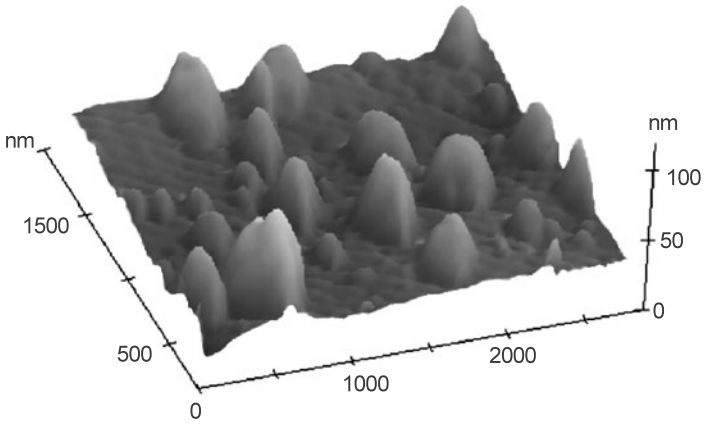

Figure 4. A spatial picture of the $CsPbCl_3$ nanocrystals on the cleavage surface of $Rb_{0.95}Cs_{0.05}Cl$–Pb crystal.

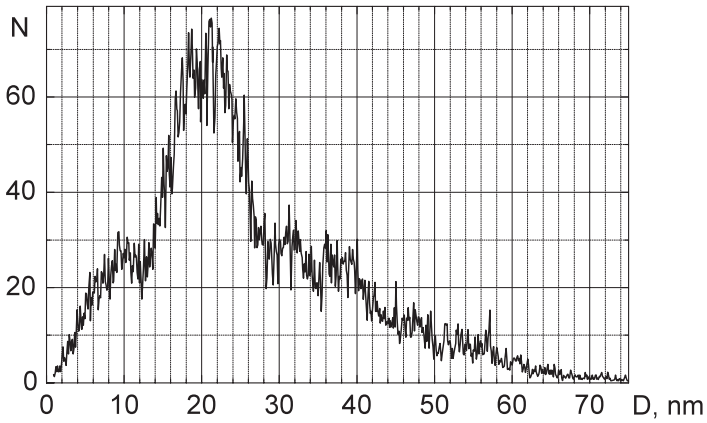

Figure 5. The statistical size distribution for $CsPbCl_3$ nanocrystals (D—diameter of the nanocrystal).

unit cell constant for $Rb_{0.95}Cs_{0.05}Cl$ solid solution is $a = 6.4$ Å. The thickness of the distorted matrix layer around the nanocrystal is just the difference between the value of the nanocrystal size obtained by AFM method and the one calculated from equation (1).

4. Conclusions

Prolonged ($t = 100$ h) high-temperature ($T = 200\,^{\circ}C$) annealing of the $Rb_{0.95}Cs_{0.05}Cl$–Pb and $Rb_{0.8}Cs_{0.2}Cl$–Pb crystals with structure of NaCl type leads to the formation of $CsPbCl_3$ nanocrystals dispersed in the corresponding matrix.

The formation of the $CsPbCl_3$ nanocrystals is confirmed by the manifestation of the quantum size effect, which shows itself as a blue-shift of the maximum of the excitonic luminescence emission of the $CsPbCl_3$ nanocrystals and a shortening of the luminescence decay time from 0.48 ns in bulk single crystal to 0.15 ns in nanocrystals ($Rb_{0.95}Cs_{0.05}Cl$ matrix). The average nanocrystal radius determined from the magnitude of the quantum size energy is 3.0 nm for $Rb_{0.95}Cs_{0.05}Cl$–Pb and 4.7 nm for $Rb_{0.8}Cs_{0.2}Cl$–Pb.

Studies of the topology of the cleavage surface of $Rb_{0.95}Cs_{0.05}Cl$–Pb crystal by the AFM method confirm the fact of lead-based nanocrystal formation.

The $CsPbCl_3$ nanocrystals embedded in wide gap matrices of $Rb_{1-x}Cs_xCl$ ($x = 0.05$–0.2) solid solution possess luminescent decay time constants in the picosecond range providing the possibility for the development of fast detectors of high-energy radiation operating at low temperature. This task demands the future study of energy transfer processes from matrix to nanocrystals under excitation in the matrix fundamental absorption range.

Acknowledgments

The authors would like to thank Professor G Zimmerer for support in measurements on the SUPERLUMI station. Partial support by INTAS (Grant 99-01350) is also gratefully acknowledged.

References

[1] Nikl M *et al* 1995 *Phys. Rev.* B **51** 5192
[2] Kondo S and Saito T 2003 *Solid State Commun.* **127** 731
[3] Myagkota S 1999 *Opt. Spectrosc.* **87** 311
[4] Voloshinovskii A, Myagkota S, Gloskovskii A and Gaba V 2001 *J. Phys.: Condens. Matter* **13** 8207
[5] Myagkota S, Gloskovsky A and Voloshinovskii A 2000 *Opt. Spectrosc.* **88** 598
[6] Kulish N R, Kunets V P and Lisitsa M P 1996 *Ukr. Fiz. Zh.* **41** 1075 (in Ukrainian)
[7] Somma F *et al* 2001 *J. Vac. Sci. Technol.* **19** 2237
[8] Nikl M *et al* 2001 *J. Phys.: Condens. Matter* **12** 1939
[9] Somma F *et al* 2001 *Radiat. Eff. Defects Solids* **156** 103
[10] Onodera Y and Toyozawa Y 1968 *J. Phys. Soc. Japan* **24** 341
[11] Nikl M *et al* 1995 *Radiat. Eff. Defects Solids* **135** 288
[12] Apanasovich V V and Novikov E G 1991 *Opt. Commun.* **78** 279
[13] Zimmerer G 1991 *Nucl. Instrum. Methods Phys. Res.* A **308** 178
[14] Belikovich B, Pashuk I and Pidzyrailo N 1977 *Opt. Spectrosc.* **42** 113
[15] Efros Al L and Efros A L 1982 *Sov. Phys.—Tech. Semicond.* **16** 1209
[16] Amitin L N, Anistratov A T and Kuznezov A I 1979 *Sov. Phys.—Solid State* **21** 3535
[17] Pashuk I, Pidzyrailo N and Macko M 1981 *Sov. Phys.—Solid State* **23** 1363
[18] Kayanuma Y and Momiji U 1990 *Phys. Rev.* B **41** 10261
[19] Voloshinovskii A, Myagkota S, Gloskovskii A and Zazubovich S 2001 *Phys. Status Solidi* b **225** 257
[20] http://www.webelements.com/webelements/elements/text/Tl/heat.html.
[21] Heidrich K, Künzel H and Treusch J 1978 *Solid State Commun.* **25** 887
[22] Bartels R A and Schule D E 1965 *J. Phys. Chem. Solids* **26** 537
[23] Tovmasian I K and Tsuzhba G M 1972 *J. Inorg. Chem.* **17** 2796 (in Russian)